Explicit Solvation Matters: Performance of QM/MM Solvation Models in Nucleophilic Addition

Jelle M. Boereboom, Paul Fleurat–Lessard, and Rosa E. Bulo*

E-mail: R.E.Bulo@uu.nl

A Multi-scale Solvation Models

In this work we employ five different models to include solvation around our NCO solute molecule. These models differ in complexity and therefore, computational cost. Here, all these methods are introduced. Their relative computational cost is discussed in the main text.

A.1 Micro-solvation Model

We use a micro-solvation model for comparison with the QM/MM methods. This model has 5 explicit water solvent molecules. In addition to that a PCM model[1] is used with a dielectric constant of 78.4 to describe the long-range electrostatic effects of water. In order to keep the explicit waters near the NCO solute molecule from diffusing into the continuum a quadratic wall (force constant of 250 kcal/mol/Å) is placed at a distance of 4.0 Å from the oxygen of the NCO molecule.

A.2 Abrupt

The most intuitive of all adaptive QM/MM methods is the `abrupt` method, where the active region is embedded in an environment region. Here, the active region is constructed by two spheres with a radius of 4.1Å around the NCO solute molecule (containing two centers; nitrogen and oxygen). All molecules within the radius of the spheres are treated QM, while the molecules in the environment region are treated with a molecular mechanics. When a molecule moves from the active to the environment region the description of the molecule changes abruptly from QM to MM.[2]

There are a few issues associated with this simple scheme. Firstly, there is a strong dependence of the potential energy on the number of electrons that are treated quantum mechanically, which may result in large 'jumps' of the total energy when a molecule enters or leaves the active region. Secondly, the position of the minimum in the potential energy surface (PES) may be different for the QM and MM description. As a consequence, after re-partitioning, a molecule might find itself far away from the minimum in the potential energy surface, leading to large 'jumps' in the forces exerted on the molecule.[2] Both of these effects mean that the `abrupt` method does not conserve energy. The energy dissipation is most severe near the QM/MM boundary leading to a heating of that particular region when not using massive thermostatting.

A.3 Difference-based Adaptive Solvation (DAS)

The origin of the problems mentioned above is the fact that there are no continuous energy or force functions describing the system when molecules move from the active to the environment region. Therefore, in order to overcome the problems associated with the `abrupt` scheme, a transition region is introduced, where molecules gradually change from pure QM character to pure MM, or vice versa. This transition region is the space between two spheres, one encompassing the active region of the `abrupt` method (radius of 4.1 Å), and the other with a larger radius of 5Å, as shown in Figure 1 of the main text.

Inside the transition region the molecules are neither fully QM nor fully MM. In order to account for this fractional QM character, multiple standard QM/MM calculations need to be performed at each time step. For each calculation there is a different partitioning of molecules that are either treated QM or MM. In Figure S1, the four partitions, that in principle contribute for the simple situation where two solvent molecules are located in the transition region, are shown. With M molecules in the transition zone, there are in principle 2^M different permutations that will contribute. Typically, M is on the order of 10, so in order to keep `DAS` calculations affordable this 2^M factor needs to be dramatically reduced. The `DAS` method uses a weightfunction $\sigma_p(\mathbf{r})$ in such a way that only $M+1$ 'ordered' partitions contribute.[3] These 'ordered' partitions are those in which all the QM molecules are closer than the MM molecules to the solute (P1,P2, and P4, Figure S1).

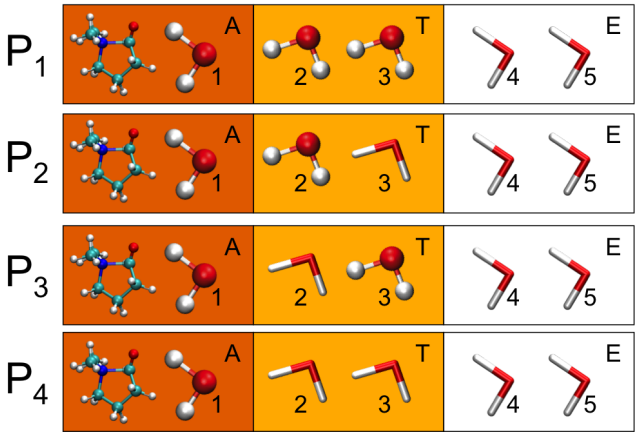

Figure S1: Four possible QM/MM partitions, with QM molecules depicted as ball and stick and MM molecules as thick lines. Partitions P1–P4 may all in principle contribute to the adaptive QM/MM energy expression, but in order to reduce computational cost only 'ordered' partitions (P1,P2, and P4), where the closest MM molecule is located further away from the center(s) than the farthest QM molecule, are calculated.

The forces exerted on the molecules in the transition region are then obtained by,

$$\mathbf{F}_{\mathrm{ad}}(\mathbf{r}) = \sum_{p}^{M} \sigma_p(\mathbf{r}) \mathbf{F}_p. \tag{1}$$

Here, $\mathbf{F}_{\mathrm{ad}}(\mathbf{r})$ is the adaptive QM/MM force vector used in the `DAS` method, $\sigma_p(\mathbf{r})$ is the weightfactor of partition p and $\mathbf{F}_p$ is the associated force vector of partition p. The weights ($\sigma_p(\mathbf{r})$) depend on the position of the solvent molecules in the transition region. So if there are two molecules in the transition region which are both close to the active region partition 1 has more weight than partition 4 (see Figure S1). The mathematical expressions for the weightfunction, $\sigma(\mathbf{r})$, can be found in Refs.[2,4]

Since, we have chosen to interpolate the forces (non-Hamiltonian adaptive QM/MM), there exists no continuous potential energy that matches them. Therefore, these simulation will not conserve the total energy, but the resulting forces will be continuous, and it is shown that they can reproduce the correct structural conformations.[2]

Until recently, energy interpolated simulations resulted in distorted structures that were caused by a 'spurious' force term originating from the gradient of the switching function. Therefore, for all practical simulations force interpolation is used. The first Hamiltonian (energy interpolation) adaptive QM/MM simulation, however, have been performed that did not result in distorted structures,[5] but those Hamiltonian simulations are beyond the scope of this work.

A.4 Buffered-force

A general problem with QM/MM calculations is that molecules that are close to the QM/MM boundary interact with both QM and MM particles, and could favor one over the other. This could lead to either an increase in density or depletion near the QM/MM boundary. The philosophy behind the buffered-force method is to address these short-ranged interactions between the QM and MM region. In order to get more accurate forces in the active region, the set of molecules which is treated by a QM description is extended, so that not only the active region, but also a finite buffer region is modeled by quantum mechanics.[6] Every time-step two independent calculations are performed: 1) A QM/MM calculation, where the active region + the buffer region are treated QM, and the environment region is treated

MM. 2) a full MM calculation on all atoms. For all the molecules in the active region the forces from the first calculation are used, while for all other molecules the MM forces are used. The advantage is that the force acting on QM molecules at the boundary come from a calculation that describes all their close neighbors also QM, and the force acting on the MM molecules come from a calculation where all their neighbors are described by molecular mechanics. This has the disadvantage that the `buffered-force` method not only has no unique potential energy, it also violates Newton's third law stating that for every action there is an equal and opposite reaction*.

Although it is possible to use a continuous transition between the QM and MM region, here we use an discontinuous transition like the `abrupt` method. For simplicity, `buffered-force` uses the same regions as `DAS`, but instead of interpolating the forces of molecules in the transition regions, this region is only used as a buffer. This means that only partition 1 (P1, Figure S1) is calculated which treats all molecules within 5Å from the nitrogen and oxygen of the NCO molecule quantum mechanically. Please note that a `buffered-force` calculation with a continuous transition region will be significantly more expensive than a `DAS` calculations, whereas (in our opinion) the results do not improve significantly, because the inherent violation of Newton's third law means that even with a continuous transition there will be significant energy dissipation near the QM/MM boundary.[3]

A.5 Flexible Inner Region Ensemble Separator (FIRES)

The `Flexible Inner Region Ensemble Separator (FIRES)` method, unlike the methods described above, is not an adaptive QM/MM method, because there is no exchange of molecules between the active region and the environment. Therefore, we classify `FIRES` as a restrictive QM/MM method. Please note that although the number of molecules in the active region is fixed, the correct density of molecules in the active region is ensured by changing the size of the active region in time.

*Please note that it is possible to ensure total momentum conservation by adding a constant value to all QM forces, so that the sum of the total forces is zero,[6] but that is not done in our current implementation.

The FIRES method uses a constraining potential (quadratic wall) that keeps the MM water molecules outside the active region. This wall is located on the circumference of a sphere around the NCO solute molecule, where the radius is given by the distance of the furthest QM molecule from the center. Therefore, the size of the active region is not constant in time, and the QM region can adjust and equilibrate to the underlying free energy surface.[3,7] Like the methods described before, also for the FIRES methods two active regions are created (that are restricted by a wall); one centered the nitrogen, one centered the oxygen of our NCO solute molecule. Since the location of the walls is determined by the outer most QM molecule of the respective regions, there is a need to assign water molecules to only one of the regions. Here, we assigned 4 solvent molecules to the region around nitrogen, and 6 (unique) waters to region around oxygen.

Although, it has been proven that FIRES simulations yield correct thermodynamic averages as long as the solvent molecules are not allowed to exchange,[7] the only way to ensure that condition is to use an infinitely steep wall. Due to integration purposes of the equations of motion, it is not possible to use such a wall as it yields ill defined forces. Consequently, even though the MM solvent molecules will feel a force resulting from the wall, the molecules will not bounce inelastically from the wall, but instead penetrate the active region to some extent. This penetration of MM molecules typically causes an aggregation of molecules near the wall. Therefore, in order to minimize the effect of this aggregation, the number of molecules in the active region should be chosen so that the average position of the wall coincides with a solvation shell peak.

A.6 Implementation of Multi-center Scheme

All the adaptive QM/MM models above are combined with a dual-center scheme, that allows two A-regions to be defined. Our implementation of multi-center adaptive QM/MM is entirely based on the work by Heyden *et al.*,[8] with a minor alteration. In single-sphere adaptive QM/MM all solvent molecules s are assigned a value $\lambda_s(a)$ based on their distance

from the QM center a. In a dual sphere approach, the corresponding λ'_s depends on the distance of the solvent molecule from all N QM centers a. Where Heyden *et al.* defined λ'_s according to,

$$\lambda'_s = \prod_a^N \lambda_s(a), \tag{2}$$

we defined λ'_s as a geometric mean,

$$\lambda'_s = \left(\prod_a^N \lambda_s(a) \right)^{1/N}. \tag{3}$$

B Metadynamics Background

MD simulations are bound to certain time-scales (typically in the picosecond to microsecond range, depending on the computational cost of the method used to evaluate the forces). Since a lot of important processes take place on longer time-scales, acceleration of the simulations is needed. Rare-event methods facilitate this acceleration. Most rare-event methods are either aimed at reconstructing the probability distribution (or the free energy) as a function of one or more coordinates (for example: Umbrella sampling,[9–12] thermodynamic integration,[13,14] parallel tempering,[15] metadynamics,[16,17] etc.). Others try to directly accelerate rare events by constructing reactive trajectories (nudged elastic band,[18] transition path sampling,[19–22] etc.). Here, metadynamics is used,[23] which allows the computation of free energy surfaces as well as acceleration of rare-events.

The metadynamics algorithm adds a biasing potential (analogue to the method by Wang and Landau[24]) to the MD simulation by placing small Gaussians along collective variables (CVs) during the simulations. These CVs are functions of the system coordinates, and are able to describe the reaction coordinate (the activated process of interest). Since the history dependent bias gradually compensates the underlying free energy surface, metadynamics simulations tend to escape from any free energy minimum via the lowest saddle point. It is

a flexible tool that allows for the computation of the free energy surface and the exploration of new reactive pathways.[25] Metadynamics is not a black-box type approach. Firstly, it is important that the collective variables are chosen appropriately, and can serve as reaction coordinate for the process of interest. Although there is no *a priori* recipe for finding the correct CVs, it is possible to check *a posteriori* if the CVs represent the reaction coordinate. Secondly, it is important to quantify the convergence of the metadynamics simulation, since this determines the accuracy of the result.[16]

B.1 Collective Variables of the Metadynamics Simulations

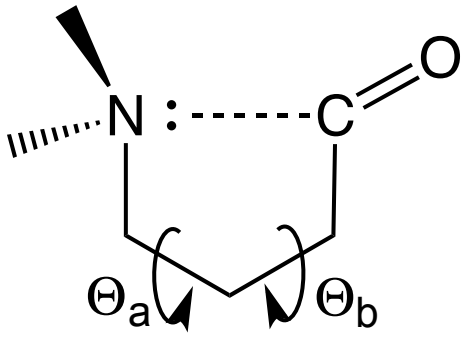

Figure S2: The structure of the NCO molecule. The first CV is the bond distance between the Nitrogen and the Carbon of the carbonyl-group, and the second CV is the combination of two dihedral angles $\sqrt{\Theta_a^2 + \Theta_b^2}$.

In Figure S2, a schematic representation of the NCO molecule is shown. In order to obtain the free binding energy of the $\mathrm{N}|\cdots\mathrm{C}^{+}-\mathrm{O}^{-}$ bond metadynamics is employed. To keep the metadynamics calculation affordable we tried to restrict the number of collective variables (CVs) to two. For the first CV we chose the bond distance between the nitrogen of the tertiary amine group and the carbon of the aldehyde. Although this first CV is enough to sample the reaction from the closed state of the NCO molecule to the open state, in order to sample the back reaction we need to actively sample the dihedral angles $\sqrt{\Theta_a^2 + \Theta_b^2}$ (Figure S2). and 2) the combination of two dihedral angles $\sqrt{\Theta_a^2 + \Theta_b^2}$ (Figure S2). Note that the back reaction can only take place when the both dihedral angles are close to 0°.

C Test of PM6-DH+

In this section details are presented on the deviations of coordinates and energies from the MP2 reference values for small molecular models of the solvated NCO molecule.

C.1 NCO Geometry

In addition to the average N|$\cdots$C and C=O distances reported in the main text, we have also calculated the root–mean–square deviation (RMSD) of the NCO molecule in order to judge the efficiency of the different class of methods (MP2, DFT with a GGA functional and Grimme's dispersion correction, and the semi-empiric PM6-DH+ functional).

Table S1: Deviation of the spatial distribution of water molecules from the MP2 reference. Listed are the ϵ_{RMSD} values of a subset of atoms; the C and O atom in the C=O moiety and all water atoms.

	ϵ_{RMSD} gas phase (Å)		ϵ_{RMSD} PCM (Å)	
n H2O	PM6-DH+	PBE-D3	PM6-DH+	PBE-D3
1	0.15	0.06	0.07	0.03
3	0.42	0.37	0.48	0.29
4	0.74	1.32	0.53	0.18

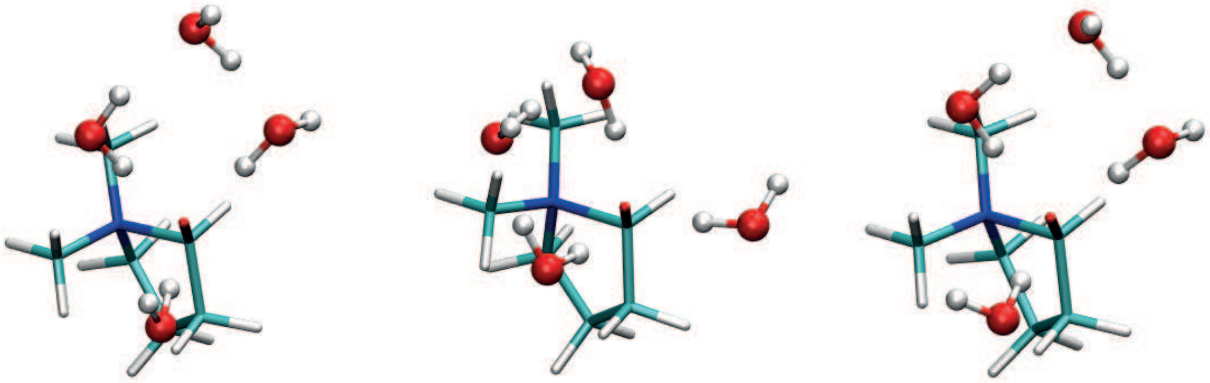

Figure S3: Spatial distribution of the water molecules after geometry optimization with MP2 (left), PM6-DH+ (middle), and PBE-D3 (right).

Qualitatively, the distribution of water molecules is barely affected by geometry optimization with different levels of theory; there are always three directly coordinated water molecules, and the fourth one forms a bridge between two others (Table S1 and Figure S3). A deviation of the coordinates of the carbonyl moiety and the water molecules from the reference van be observed, and it is larger in vacuum (PM6-DH+: 0.74 Å, PBE-D3: 1.32 Å, in the presence of 4 water molecules) than in implicit solvent (0.53 Å with PM6-DH+ and 0.16 Å with PBE-D3). We do note that the effect of the number of water molecules on the N$|\cdots$C bond (Table 3 of the main text) is much greater than the effect of fluctuating water geometries (MD simulation, Table 4 of the main text).

In solution (with 4 explicit water molecules in PCM), the solute geometry optimized with the PM6-DH+ functional has a root mean square deviation (ϵ_{RMSD}) from the MP2 reference of approximately 0.15 Å for the heavy atoms (Table S2). This PM6-DH+ error is considerably higher than the PBE-D3 value ($\epsilon_{RMSD} = 0.02$ Å). On the other hand, PM6-DH+ reproduces both the N$|\cdots$C and C=O bond-lengths extremely well in this environment ($\epsilon_{NC} = 0.01$, $\epsilon_{CO} = 0.00$, Table S2). We expect that the N$|\cdots$C and C=O bonds are most relevant to the bond-formation process under study, supporting the efficient PM6-DH+ functional as the most attractive choice for this study.

Table S2: Root mean square deviation values (ϵ_{RMSD}) of solute geometry optimized with 4 H2O and PCM; heavy atoms (left), only the two atoms in the NC bond (middle), only the two atoms in the carbonyl bond (right).

	ϵ_{RMSD} (Å)		
	heavy atoms	N$\|\cdots$C	C=O
PM6-DH+	0.152	0.009	0.003
PBE-D3	0.026	0.028	0.004

Table S3: Potential energy cost (in kcal/mol) of desorption of water molecules from the NCO molecule with four explicit water molecules. Levels of theory: MP2, DFT with the PBE-D3 functional, and the semi-empirical PM6-DH+ functional. Rows: Number of desorbed water molecules (n_d H_2O).

	gas phase			with PCM		
n_d H_2O	MP2	PM6-DH+	PBE-D3	MP2	PM6-DH+	PBE-D3
1	12.84	7.11	12.40	8.92	7.37	11.10
3	31.52	33.88	32.68	25.91	22.20	28.52
4	41.08	45.51	43.83	35.72	30.56	38.34

C.2 Potential Energies

In Table S3, the energetic cost of desorption of water molecules from the NCO molecule is listed. Overall, the desorption cost computed with PM6-DH+ is lower than the reference, while the desorption cost computed with PBE-D3 is higher. In the case of PCM solvation the average deviation of the desorption energy per water molecule from the MP2 reference is 2.37 kcal/mol with PM6-DH+ and 2.43 kcal/mol with PBE-D3.

Table S4: Potential energy barriers for the NC bond-breaking process and open minimum computed at the MP2, PBE-D3 and PM6-DH+ levels solvated with 4 explicit water molecules.

	TS		Open state	
	Barrier (kcal/mol)	d_{CN} Å	Barrier (kcal/mol)	d_{CN} Å
MP2	12.4	2.41	6.4	3.70
PBE-D3	8.5	2.62	3.8	3.79
PM6-DH+	16.5	2.64	12.4	3.78

We performed optimizations of the transition state and the open minimum all solvated with 4 explicit water molecules. The energies and CN distances obtained with PM6-DH+, MP2 and PBE-D3 (Table S4) show that the PBE-D3 barrier is lower than the MP2 reference. The PM6-DH+ barrier is higher than the reference, with approximately the same amount. The deviations from the reference are sufficiently similar with the two methods to support

our choice of PM6-DH+ to describe the system.

D Test of the Mechanical Embedding Scheme

The results in the main text are obtained using a mechanical embedding scheme. Here, we compare the Mulliken charges on the oxygen atom obtained with mechanical and electrostatic embedding calculations, using the CP2K software[26–29] with the PM6 functional (PM6-DH+ is not yet implemented). Because REAXFF does not assign fixed point-charges to the atoms it is not straightforward to use it in an EE scheme. We therefore use TIP3P/Fs charges for the MM water molecules in the electrostatic embedding computations.[30]

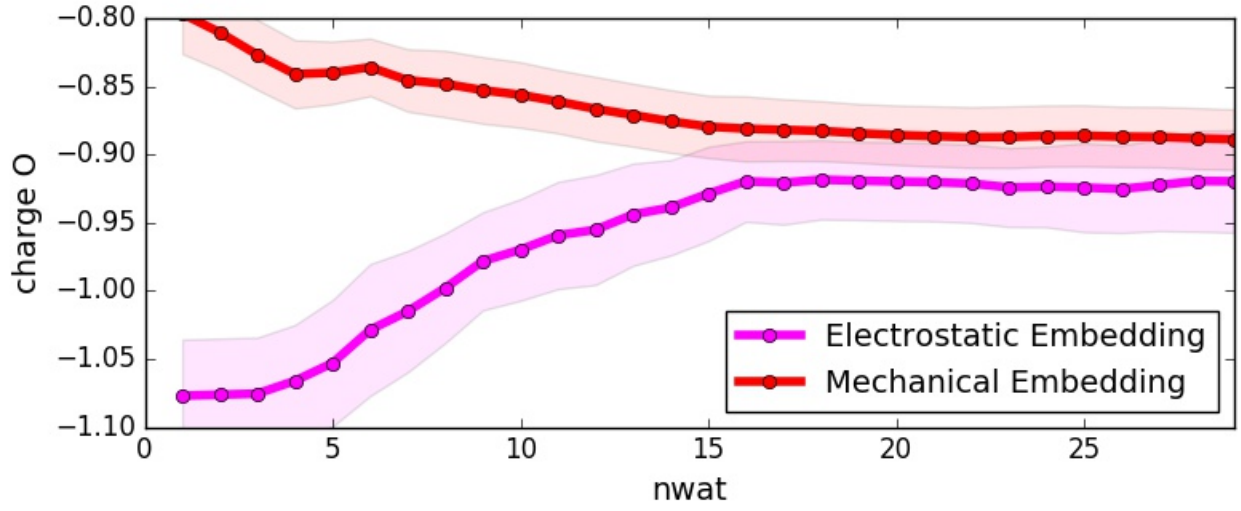

Figure S4: Convergence of PM6 Mulliken charges on the solute oxygen atom with QM-region size (nwat; number of QM water molecules) with electrostatic embedding (magenta line) and mechanical embedding (red line). The charges were computed for 50 geometries extracted from an equilibrated simulation of the closed state with the Abrupt model. The shaded area includes the standard deviation.

Electrostatic embedding exhibits behavior similar to micro-solvation (main text, Figure 3); the negative charge on the oxygen atom is overestimated when the QM region is small (Figure S4). Most notably, convergence of the electrostatic embedding charges with QM region size is no faster than convergence of the mechanical embedding charges. The converged

charges differ slightly, and based on Figure 3 of the main text, we expect that the mechanical embedding charges converge closer to the correct result. We therefore firmly believe that a mechanical embedding approach performs as well as (and possibly better than) an electrostatic embedding approach.

E Test of the Dual-sphere Adaptive QM/MM Scheme

As is illustrated in the main text, in order to properly describe the N$|\cdots$C bond breaking process, proper solvation of both the nitrogen and carbonyl group of the NCO solute molecule is needed. The most efficient way to include proper solvation near the nitrogen and carbonyl group, is to use a dual-sphere active (and transition) region centered around the nitrogen and the oxygen of the carbonyl group. When only one active region is used, the best way is to place the center of this region somewhere on the line between the nitrogen and the oxygen of our solute molecule. We have tested the efficiency of this one-sphere adaptive QM/MM model for the open state of the NCO molecule.

Our two-sphere adaptive QM/MM simulations employ fully QM active (A) regions with a radius of 4.1 Å around both the O and the N atom of our NCO solute molecule, encapsulating the entire first solvation shells. On average 14 QM water molecules reside in the two (partially overlapping) active regions, and a further 15 water molecules are located in the transition (TS) region, during metadynamics simulations. A single-sphere simulation with QM first solvation shells around the O and the N atoms requires a much larger A-region. The maximum distance between the N and the O atom along the reaction is approximately 6.0 Å, so the distance from the central point to both atoms is at most 3.0 Å. To ensure a fully QM description of all water molecules in a sphere with a radius of 4.1 Å around both the N and the O atoms, the single QM sphere around the central point must have a radius of 7.1 Å. The average number of QM and TS molecules increases dramatically for the one-sphere adaptive QM/MM approach to 58 molecules in the active region and 18 molecules in the TS

region. This means that the one-sphere adaptive QM/MM approach is significantly slower than the two-sphere approach.

We tested the timing of a single MOPAC energy computation on clusters with system sizes representative of the dual-sphere and the single-sphere approach (using a MD run of 1000 steps). The increase in the number of molecules in the QM region corresponds to a factor 6.1 increase in the timings of a single MOPAC calculation (t_{A+T}, Table S5). When the number of water molecules in the transition region increases from 15 to 18, the number of partitions computed on average increases from 16 to 19. We spread these computations over 4 cores, so the timing of a single adaptive QM/MM step should increase with a factor 7.2 (t'_{DAS}, Table S5). Because our implementation of adaptive QM/MM currently has a large overhead, the actual timing (directly comparing two QM/MM simulations using representative active and transition regions) increases only with a factor 2.5 (t_{DAS}, Table S5). The single-sphere simulations are still feasible, but considering the required length (1.25 ns), the dual-sphere approach provides a significant advantage. It is worth noting that DFT has a more unfavorable scaling than PM6-DH+ with increasing number of QM molecules, and therefore, the expected speedup of the two-sphere approach with DFT is even larger.

Table S5: Average properties of the dual sphere and the single sphere partitions along the reaction path from a DAS simulation, the number of water molecules in the A- and the T-region respectively (n_A and n_T), the time needed to compute QM forces for a system with $n_A + n_T$ water molecules (t_{A+T}), the estimated timing of a single DAS force computation, assuming no overhead (t'_{DAS}), and the computed timing for a single DAS energy and force computation with FlexMD (t_{DAS}).

	Dual sphere	Single sphere
T-region (Å)	4.1–5.0	7.1–8.0
n_A	14	58
n_T	15	18
Partitions	16	19
t_{A+T}	1.0	6.1
t'_{DAS}	1.0	7.2
t_{DAS}	1.0	2.5

All timings are normalized to the dual-sphere time.

F Test of the Micro-solvation Model

Here, we present the effect of increasing the size of the micro-solvation models from NCO and 5 water molecules (the micro-solvation model used in the main text) to NCO and 11 water molecules (to reflect the same QM size of the QM/MM solvation models), and even NCO and 23 water molecules (the maximum size of the QM/MM partition calculated for `DAS`).

Table S6: N$|\cdots$C and C=O distances of the NCO model system (left side), the average number of hydrogen bonds towards the oxygen of the aldehyde group (right side), for the different micro-solvation models studied in this work.

	N$|\cdots$C distance	C=O distance	Average number of hydrogen bonds
`Micro-solvation` (5 water)	1.63 Å	1.34 Å	3.01
`Micro-solvation` (11 water)	1.62 Å	1.34 Å	3.15
`Mirco-solvation` (23 water)	1.61 Å	1.35 Å	3.14

In Table S6, the average N$|\cdots$C and C=O bond lengths are tabulated for the different micro-solvation models. It can be seen that the N$|\cdots$C slightly decreases from 1.63 Å to 1.61 Å with the inclusion of more explicit water. Conversely, the C=O bond length increases from 1.34 Å to 1.35 Å. At the same time the average number of hydrogen bonds towards the oxygen of the NCO molecule is increased from about 3 to 3.15. While it seems that the results of the micro-solvation model are not completely converged at the size used in the main text (5 explicit water molecules), it is worth noting that the full QM reference simulation produces an average N$|\cdots$C of 1.64 Å, and that the average number of hydrogen bonds is just 2.76.

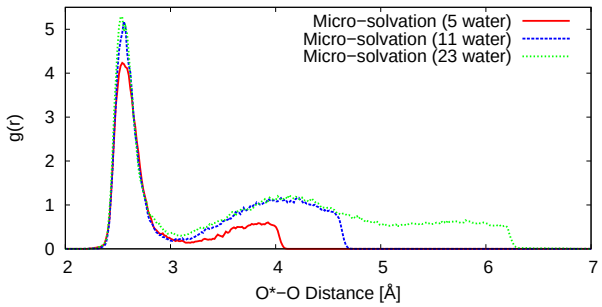

Figure S5: Radial Distribution Function (RDF) from the oxygen of the NCO molecule to the oxygens of the water solvent molecules for different micro-solvation models containing 5, 11 and 23 water molecules.

In Figure S5, the radial distribution function is plotted as a function of the NCO oxygen to the water oxygens distance. As can be seen, the first and second solvation shell of the micro-solvation models containing 11 and 23 water molecules are very similar and much higher than the solvation shells of the micro-solvation model containing 5 water molecules, and that the position of the solvation peaks are identical across the three micro-solvation models. When we compare the radial distribution of the micro-solvation models with the full QM reference, we note that they coordinate to much water in the first solvation shell. This also explains the shorter N$|\cdots$C bond length and the elevated number of hydrogen bonds in Table S6. Surprisingly, the micro-solvation model with 5 water molecules performs better than the micro-solvation models containing 11 and 23 water molecules.

F.1 Importance of Exact Location of Restraining Wall

As was mentioned in the main text, the location of the restraining wall for the micro-solvation models needs to be constructed with a-priori knowledge to ensure proper solvation. Here, we will discuss the results of a micro-solvation model containing 23 water molecules with three different location of the restraining wall: 5.8 Å, 6.0 Å, and 6.2 Å from the oxygen of the NCO solute molecule.

Table S7: N|···C and C=O distances of the NCO model system (left side), the average number of hydrogen bonds towards the oxygen of the aldehyde group (right side), for the different wall sizes for the micro-solvation model with 23 water molecules.

	N|···C distance	C=O distance	Average number of hydrogen bonds
`Wall 5.8 Å`	2.02 Å	1.32 Å	2.89
`Wall 6.0 Å`	1.61 Å	1.34 Å	3.36
`Wall 6.2 Å`	1.61 Å	1.35 Å	3.14

In Table S7, the average N|···C and C=O bond lengths and the average number of hydrogen bonded water to the oxygen of the NCO solute molecule are tabulated. The first thing to note is that the average N|···C and C=O bond length are severely affected when the restraining wall is placed at 'only' 5.8 Å from the oxygen of NCO molecule. We believe that the unreasonable high water density near the NCO molecule resulted in a spontaneous bond breaking of the N|···C bond. The average N|···C and C=O bond lengths of the micro-solvation model when the restraining wall is placed at 6.0 Å and 6.2 Å from the oxygen of the NCO molecule do not differ significantly, but the average number of hydrogen bonds are quite different.

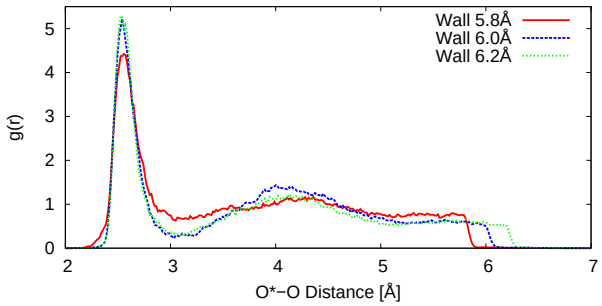

Figure S6: Radial Distribution Function (RDF) from the oxygen of the NCO molecule to the oxygens of the water solvent molecules for the micro-solvation model with 23 water molecules with changing wall radius.

In Figure S6 the radial distribution function is plotted as a function of the NCO oxygen to the water oxygens distance. Surprisingly the first solvation peak is higher for the models

where the restraining wall is placed further away from the oxygen of the NCO molecule. That means that although the water density is too high for the 5.8 Å wall model, this water does not reside in the first solvation shell. Upon further decrease of the water density (changing the wall from 6.0 to 6.2 Å), the first solvation shell remains unaltered, and only the water in the second solvation shell is diminished. Note that even for the micro-solvation model with a restraining wall at 6.2 Å from the oxygen of the NCO molecule, the first and second solvation peak are significantly higher than that of a full QM reference simulation.

G Comparison of the Solvation Models

In this section details are presented on the geometries of the closed state NCO molecule, as computed with the different solvation models.

G.1 Correlation

In order to determine the correlation between two variables, x and y, we use the following equation,

$$\rho = \frac{\sum(x_i - \langle x \rangle)(y_i - \langle y \rangle)}{\sqrt{\sum(x_i - \langle x \rangle)^2 \sum(y_i - \langle y \rangle)^2}}. \tag{4}$$

Here ρ is the correlation between the variable x and y. x_i is the value of x at step i, $\langle x \rangle$ is the average value of x, y_i is the value of y at step i, and $\langle y \rangle$ is the average value of y. ρ is a number between –1 and 1, negative numbers indicate negative correlation, 0 is non-correlation, and positive numbers indicate positive correlation.

G.2 Correlation N|···C and C=O Bond Length

The correlation between the N|···C and C=O bond length is plotted in Figure S7 for the different solvation models studied in this work. It can be seen that the spread in the N|···C and C=O bond length is quite large during the molecular dynamics runs. Nevertheless, there is a negative correlation between these two bond lengths as is tabulated in Table S8. This correlation is calculated according to Eq. (4). This correlation is a bit weaker for the restrictive QM models (`FIRES` and the micro-solvation model) than for the adaptive QM/MM models and the reference.

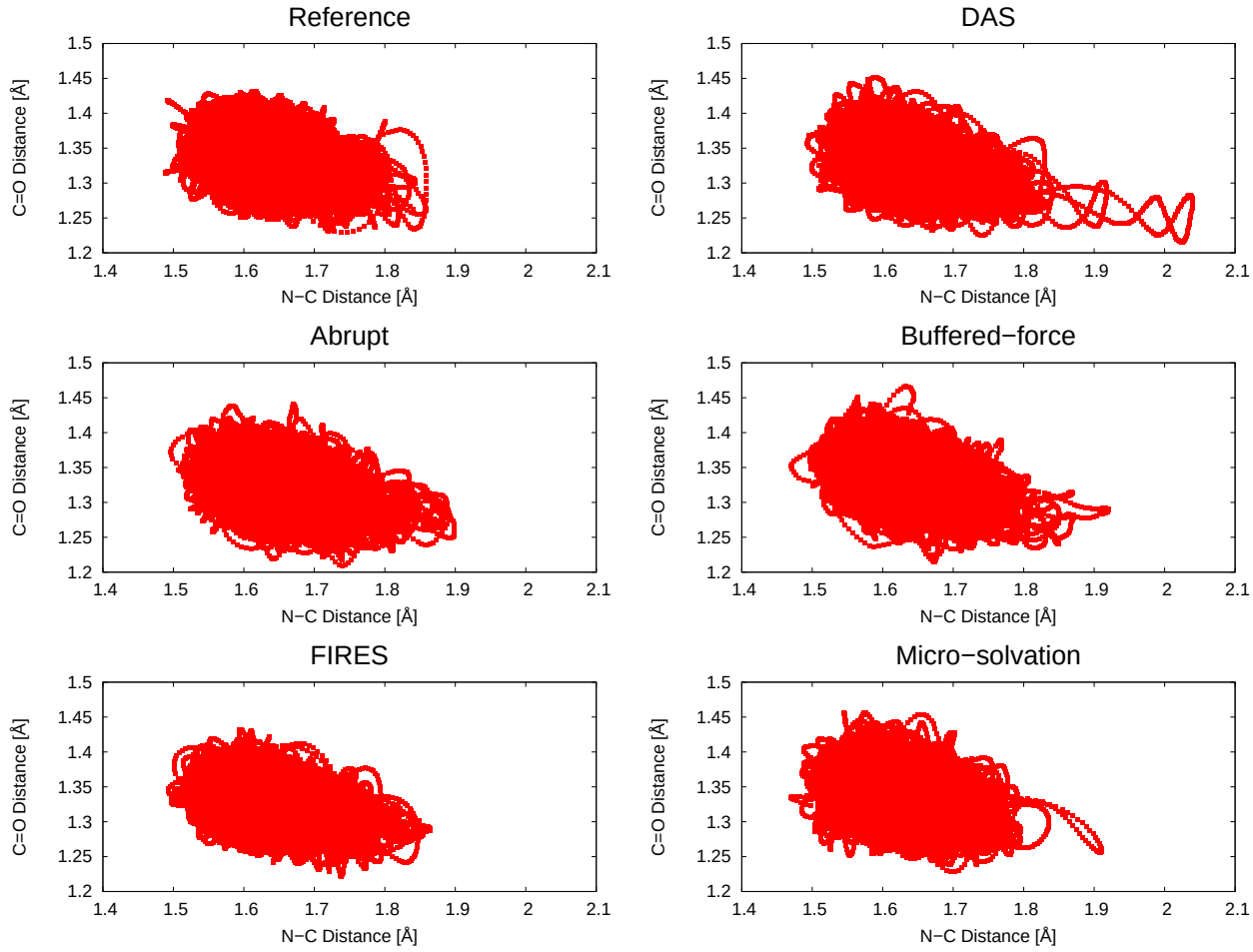

Figure S7: Correlation between the N|···C and C=O distance of the NCO molecule for the six different explicit solvation models studied in this work.

Table S8: Correlation between the N|···C and C=O distance of the NCO molecule for the six different explicit solvation models studied in this work.

	Correlation (ρ) according to Eq. (4)
`Reference`	-0.36
`DAS`	-0.37
`Abrupt`	-0.36
`Buffered-force`	-0.38
`FIRES`	-0.32
`Micro-solvation`	-0.31

G.3 Spread of the N|···C and C=O Distances

In Table 3 of the main text the average N|···C and C=O distances are tabulated for the closed state of the NCO molecule for the different solvation models used in this work. These results are obtained from molecular dynamics simulations, and have therefore, an inherent spread. In the main text, we only report the standard deviation of these results, here we also include histograms of the N|···C and C=O distances during the MD simulations.

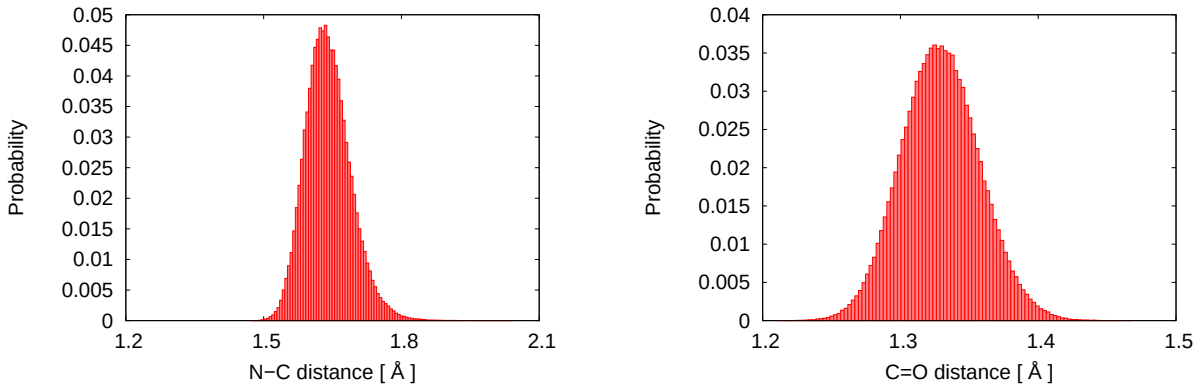

Figure S8: Histogram of the N|···C distances (left) and C=O distances (right) of the NCO molecule during the molecular dynamics simulations of the solvation models.

In Figure S8, a histogram plot can be found of the N|···C distance (left), and the C=O distance (right). It can be seen that the histograms show a unimodal distribution of both the

N|$\cdots$C and C=O distance. Moreover, the shape of the histograms suggest that the N|$\cdots$C and C=O distances are close to normally distributed.

We have chosen to use the data from all the solvation models to create Figure S8, but we have examined the histogram of the separate models as well, and found no significant difference in behavior across the different solvation models.

G.4 Solvent Structure Around the Nitrogen of the NCO Molecule

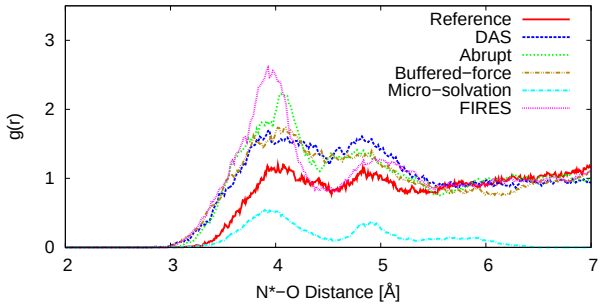

Figure S9: Radial distribution function (RDF) from the nitrogen of the NCO molecule to the oxygens of the water solvent molecules for the reference, three adaptive QM/MM methods; `DAS`, `abrupt` and `buffered-force`, and the two restrictive methods; `FIRES` and the hybrid explicit/implicit solvent model.

In Figure S9 the radial distribution function can be found from the nitrogen of the NCO solute molecule to the oxygen atoms of the water solvent molecules for all the methods, studied here. Firstly, it can be seen that the first solvation shell of nitrogen starts much later than that of an oxygen atom. Secondly, there are almost no water molecules near the nitrogen for the hybrid solvation method, indicating that this solvation model lacks solvation at most parts of the NCO molecule (except for the solvation near the oxygen of the NCO molecule, where this method was designed for). We also note that `FIRES` seems to have quite a large number of solvent molecules close to the nitrogen atom, this is caused by the restrictive walls that does not allow solvent molecules to diffuse away from the nitrogen atom. Moreover, it can be seen that RDF of `abrupt` deviates from the other two adaptive

QM/MM methods for reasons that are unclear at the moment. We do expect that the adaptive QM/MM methods have the 'best' RDFs, since there is no restriction on the solvent molecules during the simulation. Finally, we note that the RDF of the reference is quite a shallower than that of the other methods, and it does not converge to 1 at large distances. It is possible that the small box (14.1 Å) of the reference simulation is actually influencing the overall shape of its RDF.

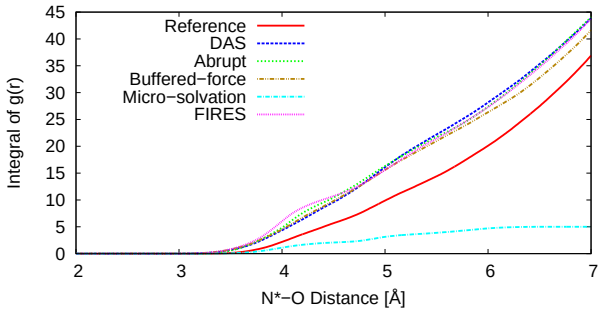

Figure S10: Integral of radial distribution function (RDF) from the nitrogen of the NCO molecule to the oxygens of the water solvent molecules for the reference, three adaptive QM/MM methods; `DAS`, `abrupt` and `buffered-force`, and the two restrictive methods; `FIRES` and the hybrid explicit/implicit solvent model.

In Figure S10, the integral of the radial distribution function of Figure S9 is shown. Firstly, as expected the micro-solvation model deviates from the other models due its design. More surprisingly, is the large difference between the reference model with the other QM/MM solvation models. We first attributed this difference to the smaller box used in the reference simulation, but this discrepancy remains even when the same (small) box is used for the QM/MM solvation models and the reference model. We now understand that the difference with the reference is mainly due to the fact that QM water is much more structured than MM water. Out of necessity, the reference simulation box is relatively small, with a radius shorter than the structural de-correlation radius. As a result, the ideal density inside the box differs from the average density of the real solution. Since the overall density in the QM reference and the QM/MM simulations is chosen the same, the QM simulation adjusts the density distribution, moving density from the first solvation shells to the furthest regions.

In summary, the discrepancy in N–O g(r) between the reference and the QM/MM simulations is not due to any artifacts of the QM/MM approach, but to the inherent difference between QM and MM, and the small size of the QM reference system. If we could perform the reference simulation in a sufficiently large box, then the differences would be reduced, but the overall difference in structure between QM and MM would still be apparent.

G.5 Local Heating with the Different Solvation Models

Table S9: Temperature of different regions of the MD simulations for the different methods under study. The active (A) region is a sphere of 4.1 Å around the central NCO molecule, for `buffered-force` and `DAS` the transition (TS) region is the space between two spheres of 4.1 and 5.0 Å around the central molecule, and the first 0.9 Å of the environment (E) is the space between spheres with a radius of 5.0 and 5.9 Å. Whereas for the `abrupt` and `FIRES` method the first 0.9 Å of the environment is the space between two spheres with radii of 4.1 and 5.0 Å around the central molecule. For `abrupt`, and `buffered-force` a Langevin thermostat was used with a friction coefficient of 0.5 a.u., whereas a friction coefficient of 0.05 a.u. was used for the `DAS` and `FIRES` methods.

	Temperature A-region	Temperature TS-region	Temperature first 0.9 Å of E	Total Temperature
`DAS`	306.11 K	302.64 K	301.10 K	300.16 K
`Abrupt`	298.24 K	NA	298.86 K	299.78 K
`Buffered-force`	300.57 K	302.98 K	294.61 K	299.87 K
`FIRES`	300.48 K	NA	301.39 K	299.59 K

In Table S9, the total temperature and local temperatures of a few important regions of the different QM/MM methods are tabulated. For QM/MM calculations it is important that the thermostat couples to all molecules, because the simulations do not conserve energy, and most of the energy is dissipated near the QM/MM boundary. When using a Nosé–Hoover thermostat, that only has one coupling to the Hamiltonian of the system, the total temperature of the system is exactly at the desired temperature, but the local temperature of the active region increases by 17 K for `DAS` to 80 K for `abrupt`, and even 119 K for the `buffered-force` method. Therefore, it is important to use a massive thermostat, so that

even regions near the QM/MM boundary are almost at the desired temperature. In this work we have chosen for a Langevin thermostat with a high friction coefficient (0.05 a.u. for `DAS` and `FIRES`, and 0.5 a.u. for `abrupt` and `buffered-force`). With these friction coefficients it is insured that no region of the QM/MM system will heat during the simulation, as can be seen in Table S9.

If `buffered-force` and `abrupt` would have the same Langevin friction as the other methods (0.05 a.u.), the local temperature would rise to 356 and 333 K, respectively.

H The N$|\cdots$C Bond Breaking Process

In this section details on the metadynamics simulations are presented, as well as statistical information on the coputed free energy barriers.

H.1 Comparing Free Energy Barriers: Welch's T-test

In order to determine whether the obtained barrier height and free binding energy of `DAS` and the micro-solvation model are significantly different we have performed the Welch's t-test, which is a variation of the Students t-test for samples with unequal variance.

The Welch's t-test defines the statistic t as,

$$t = \frac{\langle X \rangle - \langle Y \rangle}{\sqrt{\frac{s_X^2}{N_X} + \frac{s_Y^2}{N_Y}}}. \tag{5}$$

Here, $\langle X \rangle$, s_X^2 and N_X are the mean, variance and size of the first sample, and $\langle Y \rangle$,s_Y^2 and N_Y are the mean, variance and size of the second sample. The degrees of freedom (ν) associated with this variance estimate is approximated using the Welch–Satterwaite equation,

$$\nu = \frac{\left(\frac{s_X^2}{N_X} + \frac{s_Y^2}{N_Y}\right)^2}{\frac{s_X^4}{N_X^2 \nu_X} + \frac{s_Y^4}{N_Y^2 \nu_Y}}, \tag{6}$$

where $\nu_X = N_X - 1$ and $\nu_Y = N_Y - 1$.

Note that we use the Welch's t-test here, because we have an unequal variance of samples X and Y. When the sample sizes are the same (for the barrier height), the t value of the Welch's test is the same as the t value of the Students test. The number of degrees of freedom, however, is smaller.

For the barrier height: $\langle X \rangle = 12.57$, $\langle Y \rangle = 10.71$ and $s_X = 2.475$, $s_Y = 0.87$ and $N_X = N_y = 10$. This gives a statistical t of -2.249 with a degree of freedom of 11.19. The critical value of a two-sided 95% confidence interval is 2.201 for 11 degrees of freedom. Since our t is outside of that, it means that the barrier heights are significantly different for the 95% confidence interval. The free binding energies (ΔG) are much more different: $\langle X \rangle = 5.94$, $\langle Y \rangle = 9.58$ and $s_X = 1.361$, $s_Y = 1.023$ and $N_X = 7$, $N_Y = 10$. This gives a statistical t of -5.997 with a degree of freedom of 10.58, which is well outside of the critical values for the 95% confidence interval.

H.2 Metadynamics: Performance of the Collective Variables

As can be seen in Figure 6 of the main text, the opening and closing of the N$|\cdots$C bond is not instantaneous, but takes on average between 0.5 and 1 ps. This suggests that there is a slow order parameter related to the solvent structure (that was not used in the set of CVs used to bias the system). We tested the coordination number (number of hydrogen bonds) of the oxygen of the NCO molecule, but this did not change the opening and closing behavior of the N$|\cdots$C bond. We therefore expect that a more complex descriptor, involving the whole water network, plays a role. This order parameter is not slow enough to affect the final result, but only slows down the opening and closing process while the solvent adjusts. In order to avoid convergence issues, we determine the barrier height of the opening of the N$|\cdots$C bond from the deposited Gaussians when our simulations reach a N$|\cdots$C distance of 3 Å. The energy barriers for the opening of the N$|\cdots$C bond can be found in Table 5 of the main text. In order to test if the barrier height of the N$|\cdots$C bond is significantly affected

by the gradual opening and closing of the bond, we examined different criteria relating to the number of deposited Gaussians used to build up the free energy profile from which the barrier height was determined, and we tested the influence of the barrier location[†] on the barrier height. All different criteria yielded barrier heights that deviated no more than 0.3 kcal/mol within one simulation.

H.3 Metadynamics: Alternative Collective Variables

Due to the cost of metadynamics simulations, we have to limit the number of collective variables (CVs) to two. The choice of the first CV is quite straightforward; we are interested in the strength of the N|$\cdots$C bond, therefore the N–C distance is chosen. For the second CV there are two logical candidates. First, the combination of the dihedral angles of the NCO molecule (as is used in the main text) is a good choice, as active sampling of these dihedral angles is beneficial for accurate modeling of the open state of the NCO system. Second, the coordination number of oxygen is also important, as this plays a major part in the long-range effect of explicit solvation.

Here, we test the effect of using the coordination number of oxygen as a second CV on the barrier height of opening the NCO molecule. With the coordination number as second CV the barrier height of DAS becomes 10.69 kcal/mol with a standard deviation in the mean of 0.47 kcal/mol. This is almost identical to the barrier height found using the combination of dihedral angles as a second CV (10.71 kcal/mol with a standard deviation in the mean of 0.78 kcal/mol). For the micro-solvation model, the barrier height using the coordination number is 11.53 kcal/mol with a standard deviation in the mean of 0.49 kcal/mol. This deviates slightly from the results listed in the main text (12.57 kcal/mol with a standard deviation in the mean of 0.27 kcal/mol). We have performed the Welch's t-test for these values. This gives a statistical t of -1.858 with a degree of freedom of 14.12. The critical value of a two-sided 95% confidence interval is 2.145 for 14 degrees of freedom. This means

[†]Since we do not use more than 1 well in the free energy profile to obtain the barrier height, it is not possible to determine the exact barrier location.

that the t value is inside of the 95% confidence interval, that means that the difference in barrier height is not significant.

H.4 Effect Micro-solvation Model Size on Free Energy

Here, we test the effect of the number of explicit water molecules on the free energy barrier and free energy difference between the closed and open state of the NCO molecule. We compare the results for a micro-solvation model with 5 explicit water molecules (as is used in the main text) with that of a micro-solvation model containing 28 explicit water molecules.

Table S10: The barrier height ($\Delta G^{\ddagger}$) of the opening of the N$|\cdots$C bond and the binding energy (ΔG) of the N$|\cdots C^{+}-O^{-}$ interaction for the micro-solvation models containing 5 and 28 explicit water molecules. Also the standard error of the mean ($s_{\text{mean}} = \frac{s}{\sqrt{N}}$) is tabulated.

	$\Delta G^{\ddagger}$ [kcal/mol]	s_{mean} of $\Delta G^{\ddagger}$ [kcal/mol]	ΔG [kcal/mol]	s_{mean} of ΔG [kcal/mol]
DAS	10.71	0.78	5.94	0.51
Micro-solvation (5 H_2O)	12.57	0.27	9.58	0.32
Micro-solvation (28 H_2O)	14.56	0.54	6.56	1.42

In Table S10 the free energy barriers for the opening of the N$|\cdots$C bond and the free energy differences (ΔG) between the open and the closed state are listed, computed with micro-solvation models containing 5 and 28 explicit water molecules. The free energy difference ΔG obtained with the large micro-solvation model was extracted from fewer simulations than the other values, as is evident from the higher value of s_{mean} (1.42 kcal/mol). It can be seen that the barrier height obtained with a micro-solvation model with 28 explicit water molecules is 2 kcal/mol higher than that of the smaller micro-solvation model. This is in line with the results from Section F, which indicate that increasing the size of the micro-solvation cluster results in a further overestimation of the N$-$C bond. We can therefore conclude that a large micro-solvation model does not perform better than a small micro-solvation model. On the other hand the free energy difference between the open and closed state computed

with the large micro-solvation model (ΔG = 6.56 kcal/mol) is closer to the DAS value (ΔG = 5.94 kcal/mol) than the value computed with the small micro-solvation model (ΔG = 9.58 kcal/mol), although it is still too high. This is at least partially caused by a better representation of the number of hydrogen bonds towards the nitrogen of the NCO molecule in the open state. In Table S11 the average numbers of hydrogen bonded water molecules to the nitrogen atom of the NCO molecule are tabulated for the open state of the NCO molecule. With the micro-solvation model with 28 explicit water molecules an average of 0.96 water molecules is hydrogen bonded water to the nitrogen atom, which is similar to the `DAS` result (0.78). The smaller micro-solvation model only has on average 0.59 hydrogen bonded water molecules, due to the smaller explicit solvent region around only the oxygen.

Table S11: Average number of hydrogen bonded water to the nitrogen atom in the closed, transition, and open state of the NCO molecule for the micro-solvation models containing 5 and 28 explicit water molecules. Closed state: N$|\cdots$C $<$ 2.25 Å, open state: N$|\cdots$C $>$ 3.00 Å, TS state: 2.25 Å $<$ N$|\cdots$C $<$ 3.00 Å and frames from an opening or closing event are included.

	H-bonds to N		
	`Micro-solvation` (5 explicit waters)	`Micro-solvation` (28 explicit waters)	`DAS`
Open state ($>$ 3.00 Å)	0.59	0.96	0.78

In summary, the micro-solvation model with more explicit water molecules results in a more accurate free energy difference between the open and closed states of the NCO molecule. This is due to an increase in the number of hydrogen bonded water molecules to the nitrogen of the NCO molecule in the open state. The barrier computed with this large micro-solvation model, however, appears to be overestimated even more than the one computed with the small micro-solvation model, as a result of an overestimation of the N$-$C bond strength. We therefore conclude that this large micro-solvation model is not unambiguously the better choice.

I Input Structures

As mentioned in the main text all the MD simulations are performed with FlexMD, which is distributed with the ADF program package. A set of example inputs is distributed by ADF. Specific inputs are available upon request.

We do provide the optimized structures of the NCO molecule with 0,1,3 or 4 explicit waters, both in gasphase and with a PCM model as obtained with PM6-DH+ (Table 2 of the main text). Moreover, we provide the structures of 2 snapshots (one of the closed and one of the open state of the NCO molecule) of our QM/MM box (boxlength 30.804 Å), our reference box (boxlength 14.184 Å) and our micro-solvation model. These structures can be found in the compressed folder named "Structures".

References

(1) Miertuš, S.; Scrocco, E.; Tomasi, J. *Chem. Phys.* **1981**, *55*, 117 – 129.

(2) Bulo, R. E.; Ensing, B.; Sikkema, J.; Visscher, L. *J. Chem. Theory Comput.* **2009**, *5*, 2212–2221.

(3) Bulo, R. E.; Michel, C.; Fleurat-Lessard, P.; Sautet, P. *J. Chem. Theory Comput.* **2013**, *9*, 5567–5577.

(4) Jiang, T.; Boereboom, J. M.; Michel, C.; Fleurat-Lessard, P.; Bulo, R. E. In *Quantum Modeling of Complex Molecular Systems*; Rivail, J.-L., Ruiz-Lopez, M., Assfeld, X., Eds.; Challenges and Advances in Computational Chemistry and Physics; Springer International Publishing: Switzerland, 2015; Vol. 21; Chapter 2, pp 51–91.

(5) Boereboom, J. M.; Potestio, R.; Donadio, D.; Bulo, R. E. *J. Chem. Theory Comput.* **2016**, *12*, 3441–3448.

(6) Bernstein, N.; Varnai, C.; Solt, I.; Winfield, S. A.; Payne, M. C.; Simon, I.; Fuxreiter, M.; Csanyi, G. *Phys. Chem. Chem. Phys.* **2012**, *14*, 646–656.

(7) Rowley, C. N.; Roux, B. *J. Chem. Theory Comput.* **2012**, *8*, 3526–3535.

(8) Heyden, A.; Lin, H.; Truhlar, D. G. *J. Phys. Chem. B* **2007**, *111*, 2231–2241.

(9) Torrie, G.; Valleau, J. *J. Comput. Phys.* **1977**, *23*, 187 – 199.

(10) Dickson, B. M.; Legoll, F.; Lelièvre, T.; Stoltz, G.; Fleurat-Lessard, P. *J. Phys. Chem. B* **2010**, *114*, 5823–5830.

(11) Kästner, J. *WIREs: Comput. Mol. Sci.* **2011**, *1*, 932–942.

(12) Dickson, B. M.; Huang, H.; Post, C. B. *J. Phys. Chem. B* **2012**, *116*, 11046–11055.

(13) Carter, E.; Ciccotti, G.; Hynes, J. T.; Kapral, R. *Chem. Phys. Lett.* **1989**, *156*, 472 – 477.

(14) Sprik, M.; Ciccotti, G. *J. Chem. Phys.* **1998**, *109*, 7737–7744.

(15) Hukushima, K.; Nemoto, K. *J. Phys. Soc. Jpn.* **1996**, *65*, 1604–1608.

(16) Laio, A.; Rodriguez-Fortea, A.; Gervasio, F.; Ceccarelli, M.; Parrinello, M. *J. Phys. Chem. B* **2005**, *109*, 6714–6721.

(17) Bulo, R. E.; Van Schoot, H.; Rohr, D.; Michel, C. *Int. J. Quantum Chem.* **2010**, *110*, 2299–2307.

(18) Henkelman, G.; Jónsson, H. *J. Chem. Phys.* **2000**, *113*, 9978–9985.

(19) Dellago, C.; Bolhuis, P. G.; Chandler, D. *J. Chem. Phys.* **1998**, *108*, 9236–9245.

(20) Dellago, C.; Bolhuis, P. G.; Geissler, P. L. *Advances in Chemical Physics*; John Wiley & Sons, Inc., 2003; pp 1–78.

(21) E, W.; Ren, W.; Vanden-Eijnden, E. *Phys. Rev. B* **2002**, *66*, 052301.

(22) Maragliano, L.; Fischer, A.; Vanden-Eijnden, E.; Ciccotti, G. *J. Chem. Phys.* **2006**, *125*, 024106.

(23) Laio, A.; Parrinello, M. *Proc. Nat. Acad. Sci.* **2002**, *99*, 12562–12566.

(24) Wang, F.; Landau, D. P. *Phys. Rev. Lett.* **2001**, *86*, 2050–2053.

(25) Laio, A.; Parrinello, M. In *Computer Simulations in Condensed Matter Systems: From Materials to Chemical Biology Volume 1*; Ferrario, M., Ciccotti, G., Binder, K., Eds.; Lecture Notes in Physics; Springer Berlin Heidelberg, 2006; Vol. 703; pp 315–347.

(26) VandeVondele, J.; Hutter, J. *J. Chem. Phys.* **2003**, *118*, 4365–4369.

(27) Laino, T.; Mohamed, F.; Laio, A.; Parrinello, M. *J. Chem. Theory Comput.* **2005**, *1*, 1176–1184.

(28) Hutter, J.; Iannuzzi, M.; Schiffmann, F.; VandeVondele, J. *WIREs: Comput. Mol. Sci.* **2014**, *4*, 15–25.

(29) Borštnik, U.; VandeVondele, J.; Weber, V.; Hutter, J. *Parallel Comput.* **2014**, *40*, 47 – 58.

(30) Wu, Y.; Tepper, H. L.; Voth, G. A. *J. Chem. Phys.* **2006**, *124*.